JACS
JOURNAL OF THE AMERICAN CHEMICAL SOCIETY

ARTICLE

pubs.acs.org/JACS

Structure and Dynamics of Highly PEG-ylated Sterically Stabilized Micelles in Aqueous Media

Lela Vuković,[†,⊥] Fatima A. Khatib,[‡,⊥] Stephanie P. Drake,[§] Antonett Madriaga,[†] Kenneth S. Brandenburg,[§] Petr Král,[*,†,∥] and Hayat Onyuksel[*,‡,§]

[†]Department of Chemistry, University of Illinois at Chicago, Chicago, Illinois 60607, United States
[‡]Department of Biopharmaceutical Sciences, University of Illinois at Chicago, Chicago, Illinois 60612, United States
[§]Department of Bioengineering, University of Illinois at Chicago, Chicago, Illinois 60607, United States
[∥]Department of Physics, University of Illinois at Chicago, Chicago, Illinois 60607, United States

Supporting Information

ABSTRACT: Molecular assemblies of highly PEG-ylated phospholipids are important in many biomedical applications. We have studied sterically stabilized micelles (SSMs) of self-assembled DSPE−PEG_{2000} in pure water and isotonic HEPES-buffered saline solution. The observed SSM sizes of 2−15 nm largely depend on the solvent and the lipid concentration used. The critical micelle concentration of DSPE−PEG_{2000} is ∼10 times higher in water than in buffer, and the viscosity of the dispersion dramatically increases with the lipid concentration. To explain the experimentally observed results, we performed atomistic molecular dynamics simulations of solvated SSMs. Our modeling revealed that the observed assemblies have very different aggregation numbers ($N_{agg} \approx 90$ in saline solution and $N_{agg} < 8$ in water) because of very different screening of their charged PO_4^- groups. We also demonstrate that the micelle cores can inflate and their coronas can fluctuate strongly, thus allowing storage and delivery of molecules with different chemistries.

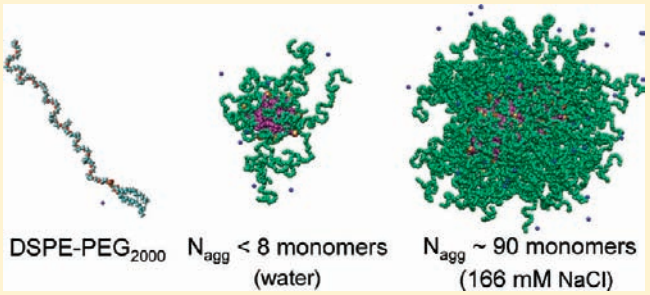

1. INTRODUCTION

Lipids, surfactants, and amphiphilic block copolymers in aqueous media can assemble into numerous stable structures, such as micelles,[1−4] disks,[5] vesicles,[6−8] and bilayers.[9−11] Poly(ethylene glycol) (PEG) lipid conjugates, assembled alone or with other lipids and cargo molecules, have broad applicability in novel biomedical formulations because of their favorable properties, such as low toxicity, biocompatibility, and ease of excretion.[12] For example, 1,2-distearoyl-*sn*-glycero-3-phosphatidylethanolamine-*N*-[methoxy(polyethylene glycol) 2000] (DSPE−PEG_{2000}) is a PEG-ylated phospholipid that is widely used in the preparation of various formulations, where the PEG layer often acts as a steric barrier that stabilizes the molecular assemblies against uptake by the mononuclear phagocytic system (MPS).[13] These formulations include micelles,[14] large unilamellar vesicles,[15,16] lipid-protected particles, and immunoliposomes for gene delivery;[17−19] coated carbon nanotubes for near-IR imaging;[20] biologically functional surfaces;[21] and ultrasound contrast agents.[22,23] Many DSPE−PEG_{2000}-based nanostructures play an important role in the development of pharmaceutical drug delivery systems.[13,24−26] For example, DSPE−PEG_{2000} is used as a component of the U.S. FDA-approved pharmaceutical product Doxil.

We previously studied sterically stabilized micelles (SSMs) of self-assembled DSPE−PEG_{2000} as biocompatible and relatively nontoxic drug delivery nanocarriers.[27] SSMs have a hydrophobic core, an ionic interface, and a semipolar palisade PEG layer, all of which can serve as platforms for association of hydrophobic and amphiphilic drugs and peptides.[28,29] We experimentally characterized simple and mixed SSMs with respect to shape, core polarity, and aggregation number (N_{agg}) in HEPES-buffered saline (pH 7.4).[30,31] Understanding the structure and the dynamics of the self-assembled DSPE−PEG_{2000} monomers in different aqueous media is crucial for the optimization of SSM systems for drug delivery and other potential applications. Micellar aggregates are known to have different equilibrium sizes, critical micelle concentrations (CMCs), and aggregation numbers[32] in solutions having different ionic strengths and monomer concentrations.[33] These parameters play a crucial role in the applicability of the PEG-ylated lipid micelles.

In this work, we experimentally characterized SSMs in terms of size, solution viscosity, and CMC both in pure water and in an isotonic salt solution, represented by HEPES-buffered saline. To understand the experimental results in molecular detail, we carried out large-scale atomistic molecular dynamics (MD) simulations of the DSPE−PEG_{2000} assemblies in water and saline solutions. We examined how the solvent type and lipid concentration affect the equilibrium structure and dynamics (fluctuations) of SSMs and the physical properties of their solutions. Although various micelles have been modeled in the past,[34−39] to the best

Received: May 2, 2011
Published: July 22, 2011

dx.doi.org/10.1021/ja204043b | J. Am. Chem. Soc. 2011, 133, 13481–13488

of our knowledge, this is the first study to model highly PEGylated micelles using atomistic MD simulations and reveal their characteristics in atomistic detail.

2. MATERIALS AND METHODS

2.1. Sample Preparation. We dissolved DSPE−PEG_{2000} in either pure water or 10 mM HEPES-buffered saline (pH 7.4) at monomer concentrations of c = 5−40 mM. All samples were vortexed, sonicated, and flushed with argon and then equilibrated for 4 h in the dark at room temperature (T = 25 °C).

2.2. Characterization of Experimental SSM Solutions. Aqueous solutions of SSMs were analyzed to determine the mean particle diameter, solution viscosity, and CMC. Particle sizes in the SSM dispersions were measured using both a dynamic light scattering (DLS) particle sizer (Agilent 7030 NICOMP DLS/ZLS) equipped with a 100 mW He−Ne laser at 632.8 nm set up at an angle of 90° and a Brookhaven instrument with three major components (a BI-200SM goniometer and BI-9000AT digital correlator from Brookhaven Instruments and a Lexel 95 3 W argon ion laser at 514.5 nm from Lexel Inc.) set up at angles of 30, 90, and 120°. The viscosities of the SSM dispersions were measured using Brookfield DV-II+ programmable viscometer (cone/plate) with a CPE-42 spindle (cone) at a chamber temperature of 25 °C. The CMC of SSMs in pure water was determined using 1,6-diphenyl-1,3,5-hexatriene.[14] Further experimental details and the sources of all chemicals used are available in the Supporting Information.

2.3. Molecular Dynamics Simulations. We performed atomistic MD simulations of micelles composed of DSPE−PEG_{2000} monomers with sodium counterions using the NAMD package[40] and the CHARMM27 force field (C35r revision for ethers).[41,42] Micelles with various aggregation numbers (N_{agg} = 8−90) were modeled in pure (TIP3P) water and in 0.166 M NaCl solutions. The ionic strength of the NaCl solution was matched to the ionic strength of the buffer solution used in the experiments. The systems were equilibrated in the *NPT* ensemble at P = 1 bar and T = 300 K. Further details concerning the MD simulations are provided in the Supporting Information.

3. RESULTS AND DISCUSSION

3.1. Experimentally Observed Micelle Sizes. In Figure 1, we show the observed intensity-weighted size distributions and average hydrodynamic diameters (d_h) of the experimentally prepared DSPE−PEG_{2000} assemblies equilibrated in water (a−e) and ionic solution (f−j) as described above. As the monomer concentration increased from 5 to 40 mM, the d_h values of SSMs in water observed using the NICOMP instrument at the 90° angle slowly increased from ∼4.1 to 5.6 nm, while those observed using the Brookhaven instrument at the 90° angle increased from ∼2.2 to 4.0 nm. The differences in the results obtained using the two instruments at low concentrations (c = 5−20 mM) may be due to the fact that DLS measurements are less reliable when the particles are smaller than 5 nm in diameter (instrument documentation). At these extremely small sizes, the Brookhaven instrument might average over the peaks of the 4−5 nm micelles and the 1−2 nm monomers (and impurities) that appear in the NICOMP data. Nevertheless, the trend of a slow increase in SSM size in water with increasing monomer concentration (observed using both instruments) is expected to hold. This size dependence may be caused by the fact that the effective ionic strength of the solutions (micelle screening) increases with the monomer concentration as the monomer counterions become crowded in the limited space between the micelles (see the Figure 4 inset).

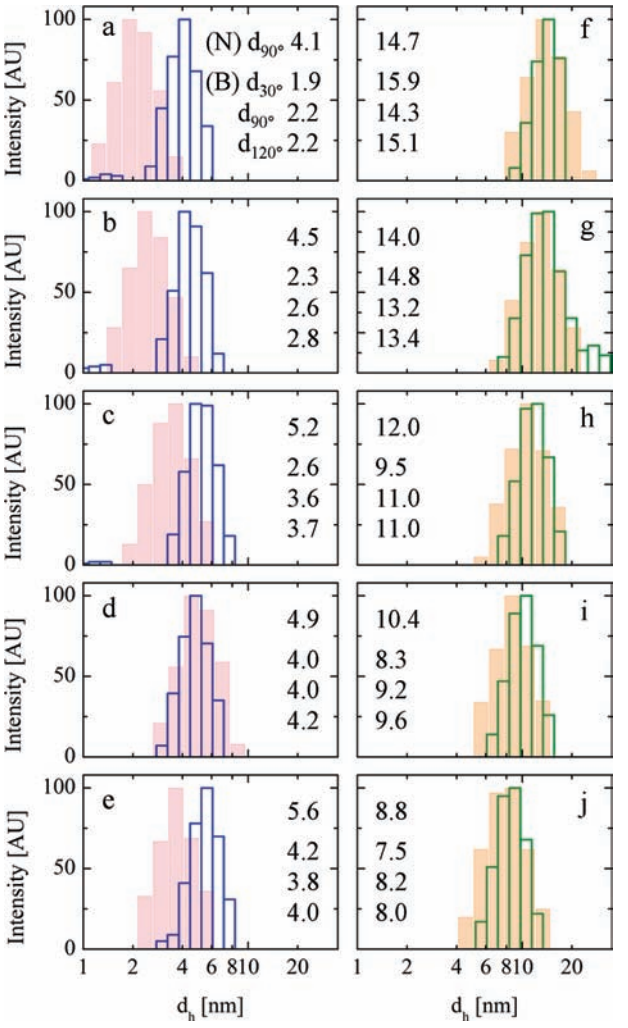

Figure 1. Experimental intensity-weighted size distributions of SSMs: (left) in pure water at concentrations of (a) 5, (b) 10, (c) 20, (d) 30, and (e) 40 mM; (right) in HEPES-buffered saline at concentrations of (f) 5, (g) 10, (h) 20, (i) 30, and (j) 40 mM. Line histograms show data obtained using the NICOMP instrument at the 90° angle, and shadow histograms show data obtained using the Brookhaven instrument at the 90° angle. Average hydrodynamic diameters (d_h) obtained using the NICOMP instrument (N) at the 90° angle and using the Brookhaven instrument (B) at the 30, 90, and 120° angles are shown in each plot.

In ionic solutions, the observed micelles always had narrow size distributions whose peaks shift from $d_h \approx$ 15 nm at c = 5 mM to d_h = 8 nm at c = 40 mM (Figure 1f−j). Previously, Johnsson et al.[43] studied DSPE−PEG_{2000} aggregates in 0.15 M NaCl aqueous solutions at lipid concentrations of 0.4−7 mM. The aggregation numbers and hydrodynamic radii of their DSPE−PEG_{2000} micelles in these media are similar to our observations in HEPES-buffered saline at c = 5 mM.[14] This indicates that the presence of ions is of great importance for the micelle sizes and aggregation numbers.

In Figure 1, we also show the average hydrodynamic diameters for SSMs in all of the studied solutions as obtained by the NICOMP instrument at the 90° angle and the Brookhaven instrument at the 30, 90, and 120° angles. The average values of d_h obtained by the Brookhaven instrument at different angles are

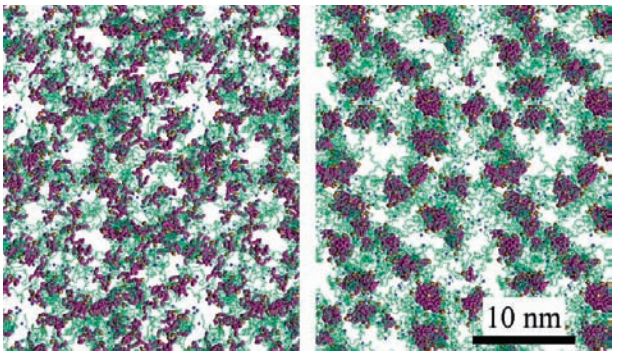

Figure 2. Formation of DSPE−PEG_{2000} micelles in water at the monomer concentration c = 40 mM (left) at the beginning of the assembly and (right) after 30 ns of equilibration at T = 300 K. The average first-neighbor SSM core−core distance is $d_{C-C} \approx 7$ nm. The projected images show slices of the aqueous solutions that are 18.7 nm in width.

similar, since the angular dependence of the scattering of 632.8 nm light by particles with d_h < 25 nm is very small (instrument documentation).

3.2. Simulations of DSPE−PEG_{2000} Monomer Self-Assembly in Water. In order to understand the observed behavior of DSPE−PEG_{2000} in water, we first simulated the formation of SSMs from hydrated DSPE−PEG_{2000} monomers. Initially, randomized monomers with c = 40 mM were hydrated at T = 300 K, as shown in Figure 2 (left). From this configuration, the system developed within 30 ns into an assembly of small micelles with N_{agg} < 11, as shown in Figure 2 (right). At c = 40 mM, neighboring SSMs often came in contact through their extended PEG coronas. Although the system was not yet equilibrated at 30 ns, these results showing the stabilization of small micelles support the data observed in Figure 1a−e.

3.3. MD Simulations of Equilibrated Micelles. In order to better understand the experimentally observed results, we simulated individual equilibrated molecular aggregates formed by various numbers of DSPE−PEG_{2000} monomers in water and ionic solution. In Figure 3a−e, we show micelles formed by 8, 10, 15, 20, and 50 DSPE−PEG_{2000} monomers equilibrated in water for 5−16 ns. In our analysis below, we focus on the 10-monomer SSM in water, whose size is in rough agreement with the SSM sizes observed in water using both DLS instruments for monomer concentrations c > 30 mM. For comparison, we show in Figure 3f a 90-monomer micelle equilibrated in the 0.166 M NaCl solution for 10 ns. The 90-monomer estimate used in the preparation of this micelle was based on our small-angle neutron scattering (SANS) measurements of SSMs in HEPES-buffered saline at c = 5 mM.[14,30]

3.3.1. Structure and Dynamics of the Micelle Core. In all of the equilibrated micelles, we can recognize three unique regions: the core, the ionic interface, and the PEG corona. The micelle cores in Figure 3a−f, which are formed by aggregated alkane blocks, are shown in the same order in Figure 3g. At smaller aggregation numbers, the micelles reorganize on subnanosecond time scales, and their cores gain a spherical shape. Larger micelles (N_{agg} > 20) reorganize in several nanoseconds, and their cores become more ellipsoidal. This is particularly clear in the case of the 90-monomer micelle formed in ionic solution, whose core has an oblate shape (the lengths of the three principal axes are ∼3.0 nm, ∼3.5 nm and ∼2.0 nm, giving the aspect ratio of ∼1.7), in agreement with our

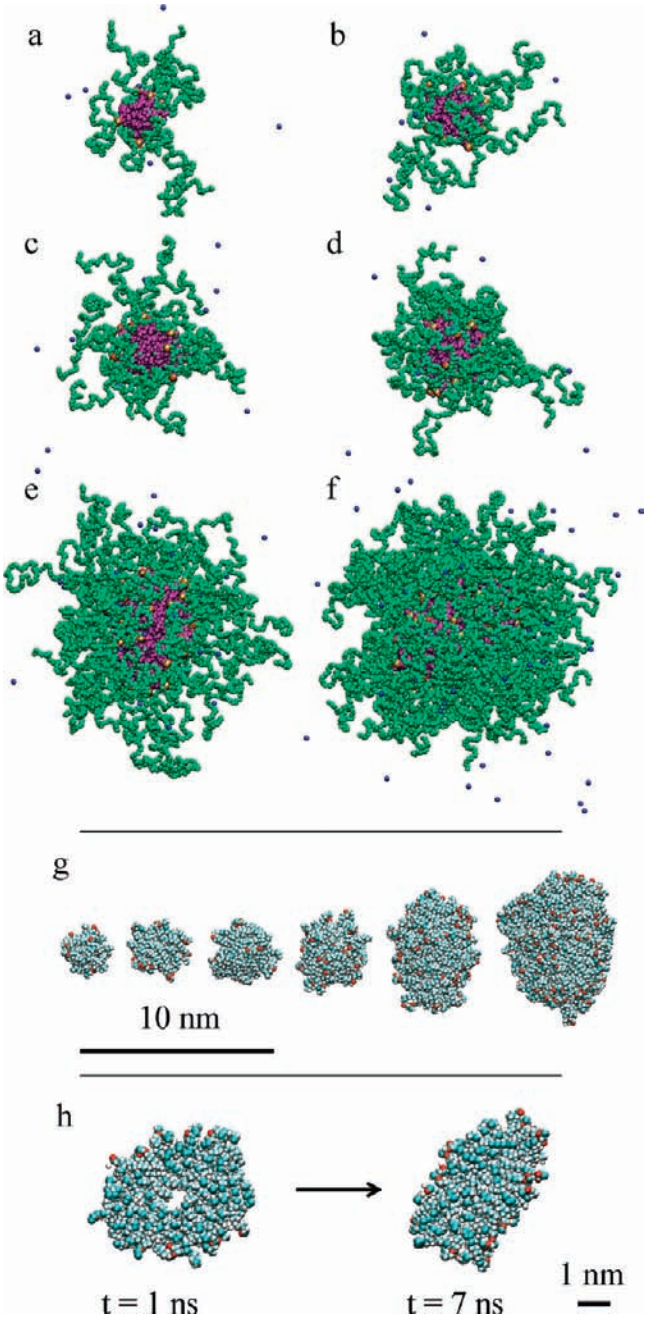

Figure 3. Snapshots of equilibrated micelles (T = 300 K) with (a−e) N_{agg} = (a) 8, (b) 10, (c) 15, (d) 20, and (e) 50 in water and (f) N_{agg} = 90 in 0.166 M NaCl solution. (g) Equilibrated alkyl cores of the micelles in (a−f) shown in the same order. Water molecules have been omitted for clarity. Images (a−g) are shown using the same scale [the scale bar is shown in (g)]. (h) Relaxation of the 90-monomer SSM core in 0.166 M NaCl solution, shown on a 1 nm thick cross section.

previous measurements of SSMs with the aggregation number of N_{agg} ∼93, obtained by SANS using a low-Q diffractometer.[30]

It is of great importance to understand the dynamical reorganization of the SSM core. In Figure 3h, we show two snapshots of the 90-monomer SSM core as it relaxes from the initial spherical shape with a vacancy in the center (hollow) to the oblate shape (splashed). The hollow core might carry drugs and other molecular or nanoparticle cargo, as observed in experiments.[28,31]

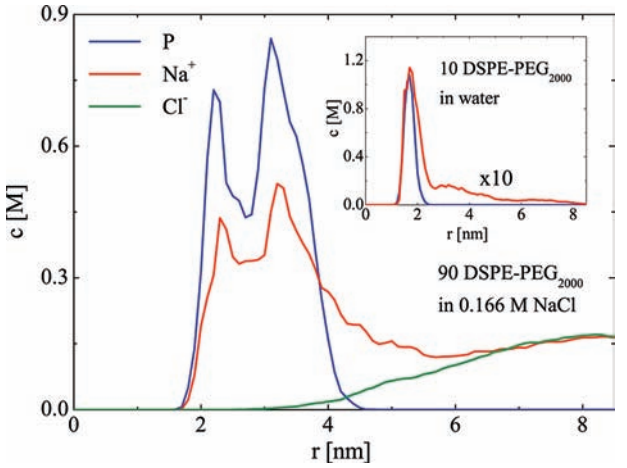

Figure 4. Molarities of P atoms (in the PO_4^- groups on the DSPE−PEG_{2000} monomers) and Na^+ and Cl^- ions as functions of the radial coordinate r with respect to the SSM center of mass for 90-monomer SSM in 0.166 M NaCl solution. The inset shows the molarities of P atoms and Na^+ ions for the 10-monomer SSM in water.

The filled SSM with the more spherical core might become more stable.

3.3.2. Structure and Dynamics of the Ionic Interface. The cores of all of the SSMs are covered by the charged phosphate groups (PO_4^-) from the DSPE−PEG_{2000} monomers, which are screened by the Na^+ counterions freely present in our (neutral) systems. Screening of the ionic interface is of great importance for micelle stabilization, as discussed in detail later. In Figure 4, we show the molarities of the ionic species present in the 90-monomer SSM in 0.166 M NaCl solution and the 10-monomer SSM in water (inset) as functions of the radial distance from the micelle center. In the 10-monomer SSM, the distribution of the PO_4^- groups has a single peak localized at $r \approx 1.7-1.8$ nm, reflecting the spherical shape of the core. In the 90-monomer SSM, the core has an oblate shape, resulting in two peaks for the PO_4^- groups localized at $r \approx 2.2$ and 3.1 nm. In both cases, the PO_4^- groups are largely screened by the Na^+ counterions in the Stern layer, located in the region of the PO_4^- groups. The resulting diffuse ionic atmosphere[32] maintains the neutrality of the whole molecular complex. In Figure 4, we can see that in water, the neutrality is achieved within 4−6 nm of the PO_4^- groups, while in the ionic solution, it is achieved within 2−3 nm because of the short screening length ($\lambda \approx 0.75$ nm). The Na^+ concentration approaches the bulk value of either zero (water) or 0.166 M, where in the latter case the Cl^- concentration also increases to the same bulk value. The Stern and diffuse ion layers complete the charge double-layer region, which permeates the PEG corona.

3.3.3. Structure and Dynamics of the Micelle Corona. The local density and conformations of PEG chains forming the SSM corona also depend on N_{agg}. As shown in Figure 3a−f, the PEG chains in all of the studied SSMs can transiently form clumps or remain isolated. We analyzed the chain dynamics in more detail for the 10-monomer SSM in water (Figure 3b) and the 90-monomer SSM in 0.166 M NaCl solution (Figure 3f).

In Figure 5, we show equilibrium fluctuations of d_{PEG}, the local PEG thickness in the micellar PEG corona, as a function of the inclination angle θ and the azimuthal angle ϕ (in spherical coordinates with the origin at the SSM center of mass). Figure 5a−d shows that in the 10-monomer SSM, a large fraction (~30%) of the core

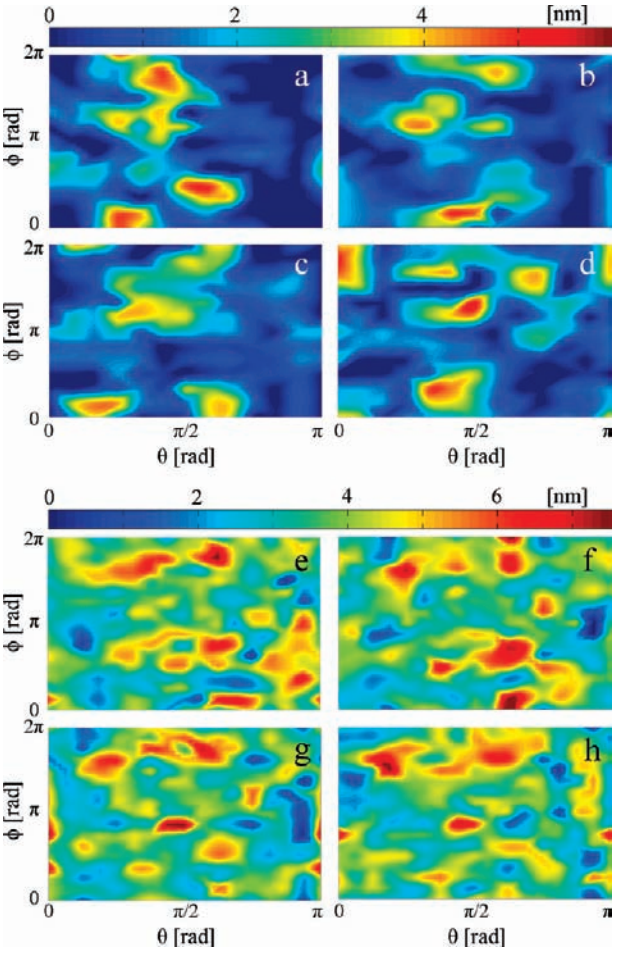

Figure 5. Local thicknesses of the PEG corona (d_{PEG}) for (a−d) the SSM with $N_{agg} = 10$ in water at (a) 3, (b) 6, (c) 10, and (d) 16 ns and (e−h) the SSM with $N_{agg} = 90$ in 0.166 M NaCl solution at (e) 7, (f) 8, (g) 9, and (h) 10 ns as functions of the inclination angle θ and the azimuthal angle ϕ.

is always fully exposed to water. We can see in the four snapshots taken at 3, 6, 10, and 16 ns that most of the PEG chains fluctuate but remain folded at the core, while one or two chains can occasionally protrude away from the core ($d_{PEG} > 5$ nm).

In Figure 5e−h, we show the fluctuations of d_{PEG} in the 90-monomer SSM in 0.166 M NaCl during a 3 ns trajectory. The large SSM has a more homogeneous PEG corona, which occasionally exposes the core to the aqueous solution. Here only <10% of the hydrophobic core is always exposed to water. The corona fluctuations create pockets with different chemistries that might be able to carry molecular cargo, such as drugs and peptides.

In Figure 6, we show the average density distributions $\rho(r)$ for the hydrophobic core groups, the PEG corona groups, and water for the 10-monomer SSM in water and the 90-monomer SSM in 0.166 M NaCl solution. The densities were calculated using the equation

$$\rho(r) = \frac{1}{N_t} \sum_{t=1}^{N_t} \sum_{i=1}^{N_a} \frac{m_i}{V} \quad (1)$$

where m_i is the mass of the ith atom in the set of N_a atoms found in the bin with volume V (each bin is a spherical shell with thickness $\Delta r = 1$ Å centered at the SSM center of mass). The averaging was performed over $N_t = 2000$ frames during 4 ns

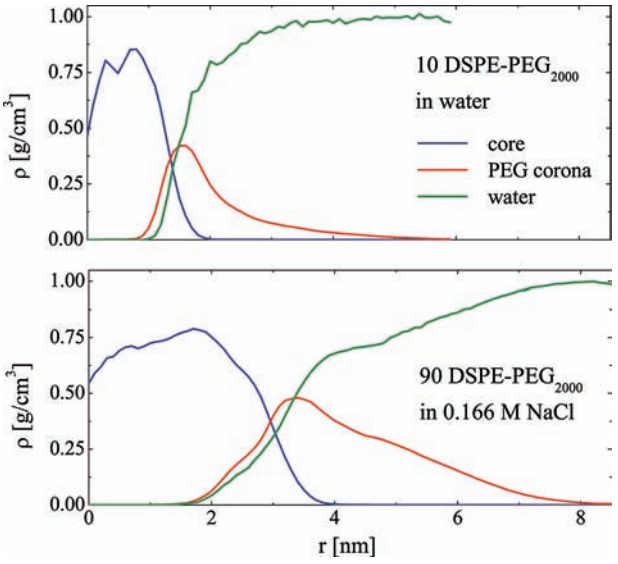

Figure 6. Density distributions as functions of the radial coordinate r with respect to the SSM center of mass for (top) the 10-monomer SSM in pure water and (bottom) the 90-monomer SSM in 0.166 M NaCl solution. The core and PEG distributions were averaged over the last 4 ns of the simulations, while the water distribution was averaged over the last 0.1−0.2 ns.

simulations for the core and PEG and over N_t = 5−10 frames during 0.1−0.2 ns simulations for water.

In the 10-monomer SSM (Figure 6 top), the hydrophobic core has a relatively sharp boundary at $r \approx 1.7-1.8$ nm. This is followed by the PO_4^- groups and a narrow PEG layer with a thickness of $\Delta_{PEG} \approx 1.5$ nm. The individual PEG chains are highly coiled and have "mushroomlike" conformations, as observed on flat surfaces (membranes) at low PEG densities.[44] Water also fills the space between the PEG chains, as shown by its distribution.

The 90-monomer SSM (Figure 6 bottom) has a rather different structure of its layers because the oblate core terminates at $r \approx 2.5-4$ nm. The onset of the PEG layer is broader than in the 10-monomer SSM as a result of the core ellipticity. The congested PEG chains have more "brushlike" conformations, as seen on flat surfaces in the limit of high surface coverage.[44] The average thickness of the PEG corona ($\Delta_{PEG} \approx 3.8$ nm) is in good agreement with the value of $\Delta_{PEG} \approx 3.5$ nm found for DSPE−PEG_{2000} micelles in 0.15 M NaCl solution.[43] Water again fills the space between the PEG chains.

3.4. Comparison of the Experimental and Theoretical Micelle Sizes. In Table 1, we show the effective diameters of the equilibrated micelles and their cores (d_{tot} and d_{core}, respectively). These values were obtained by angular averaging (2−5 ns) of the maximum radial extensions of the PEG chains ($r_{max,tot}$) and core groups ($r_{max,core}$) with respect to the SSM center of mass:

$$d_{tot/core} = \frac{2}{N_t N_\theta N_\phi} \sum_{t=1}^{N_t} \sum_{\theta=1}^{N_\theta} \sum_{\phi=1}^{N_\phi} r_{max,tot/core}(\theta, \phi, t) \qquad (2)$$

Here the averaging was performed on a spherical grid with N_θ = 10 bins for the inclination angle θ and N_ϕ = 20 bins for the azimuthal angle ϕ over the selected number of frames, N_t = 1000−2500 for 2−5 ns trajectories.

Comparison of the theoretical effective sizes d_{tot} with the experimental hydrodynamic sizes d_h shown in Figure 1 indicates

Table 1. Dependence of the Micelle Diameter (d_{tot}) and Core Diameter (d_{core}) on the Aggregation Number N_{agg}[a]

N_{agg}	8(a)	10(b)	15(c)	20(d)	50(e)	90(f)	10	15
d_{tot} [nm]	5.9	6.0	7.3	7.7	11.8	13.9	6.3	6.9
d_{core} [nm]	2.3	2.5	2.9	3.4	4.6	6.3	2.5	2.9

[a] The labels (a)−(f) correspond to those in Figure 3; the last two systems were simulated in 0.166 M NaCl solution, as in the case of (f).

that micelles observed in pure water with diameters of $d_h \approx$ 4−5 nm should contain $N_{agg} < 8$ monomers. We should keep in mind that the two definitions of micelle sizes are different, which can make this comparison unreliable, especially at small sizes of the aggregates with distantly protruding individual chains (see Figure 3 a). SSMs with $N_{agg} \leq 8$ were also observed in our simulations of 40 mM DSPE−PEG_{2000} solution (Figure 2 right). On the other hand, in the buffered solutions, the experimental SSM sizes were always $d_h > 8$ nm (Figure 1 bottom), indicating $N_{agg} > 20$. At the DSPE−PEG_{2000} monomer concentration of c = 5 mM in buffer,[14,30] the experimentally observed SSMs have $N_{agg} \approx 90$ and $d_h \approx 15$ nm. This diameter is in close agreement with the d_{tot} value of 13.9 nm obtained for the modeled 90-monomer SSM (Figure 3f and Table 1).

In the last two columns of Table 1, we also present the calculated sizes of 10- and 15-monomer micelles in the 0.166 M NaCl solution. This ionic strength matches that of the buffer solution in which stable micelles with N_{agg} = 90 were formed at c = 5 mM. The simulated small micelles (10−15 monomers) acquire very similar sizes in water and the NaCl solution. This indicates that the experimental SSM sizes are determined by their N_{agg} values rather than different arrangements of the monomers.

3.5. Effect of the Ionic Concentration on the Micelle Sizes. When ionic lipid and surfactant micelles are assembled in ionic solutions, the overall large number of counterions provides better screening of the charged headgroups. This results in reduced repulsion of the headgroups, eventually leading to stabilization of more monomers in each assembled structure.[45,46] On the other hand, in micelles assembled from nonionic (neutral) monoalkyl-PEGs, the aggregation number increases only slightly when the salt concentration is increased (up to c = 1.3 M).[47]

The micelle morphology can be also influenced by the nature of the headgroups. Ionic (DSPE−PEG_{2000}) and nonionic (monoalkyl-PEGs, DS-PEG_{2000}, and DSG-PEG_{2000}) PEG-ylated monomers all assemble into globular micelles.[47,48] However, when the PEG-ylated polymers have headgroups with attractive interactions, the monomers can form aggregates with different morphologies. For example, lipids with one to four 16-carbon acyl chains connected by amide groups to PEG_{2000} tend to form fibrous structures in water[49] as a result of hydrogen bonding between the amide groups.

The fact that the aggregation numbers in our SSMs are larger in ionic solution than in pure water is likely related to the enhanced screening of the charged and aggregated PO_4^- headgroups by abundant free counterions from the ionic solution.[45,46] To clarify this possibility, we theoretically examined how 10-monomer PEG-ylated micelles in water and 0.166 M NaCl solution are screened by the ion distributions formed around the ionic PO_4^- groups.

In Figure 7 (top), we show the average number of Na^+ and Cl^- ions (N) at various distances r from the P atoms in DSPE−PEG_{2000} monomers. These data were obtained by integrating the P−Na^+ and P−Cl^- radial distribution functions (RDFs) using Visual

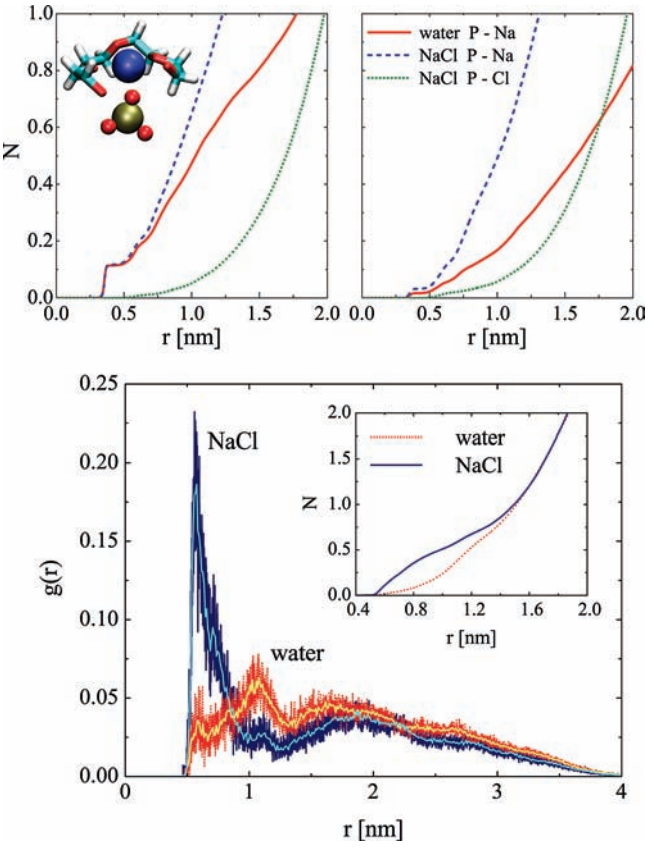

Figure 7. (top) Average numbers of Na^+ and Cl^- ions (N) as functions of the distance r from phosphorus atoms of DSPE−PEG_{2000} monomers in 10-monomer micelles in water and 0.166 M NaCl solution. The data were obtained by integration of the radial distribution function $g(r)$ between P and Na^+ or Cl^-. Plots were obtained from (left) a trajectory where one of the Na^+ ions is trapped by a PEG chain close to the PO_4^- group (inset) and (right) a trajectory where all of the ions are free. (bottom) Normalized RDFs $g(r)$ for phosphorus atoms on different DSPE−PEG_{2000} monomers in 10-monomer micelles in water and in 0.166 M NaCl solution. Plots of the average numbers of phosphorus atoms (N) within a distance r of another phosphorus atom are shown in the inset.

Molecular Dynamics (VMD).[50] In these calculations, we found that Na^+ counterions can assume metastable configurations in PEG pockets around the PO_4^- groups, as shown in the inset of Figure 7 (top left). Since these configurations transiently occur only in some of the trajectories, we separately show in Figure 7 the plots for the trapped (top left) and free (top right) Na^+ configurations. In both Na^+ configurations, the integrated RDFs always show more positive counterions surrounding the negative PO_4^- group in ionic solution than in pure water. Moreover, at short distances from the phosphorus atoms ($r < 0.7$ nm), the average number of Na^+ ions is observed to be larger when the ions are trapped.

In Figure 7 (bottom), we show normalized RDFs [$g(r)$] of phosphorus atoms from different DSPE−PEG_{2000} monomers for the 10-monomer micelles equilibrated in water and ionic solution. In both cases, trajectories with trapped Na^+ conformations were used. The first peaks in $g(r)$, observed at $r < 1$ nm, are 8 times smaller in water than in the ionic solution. In the inset of Figure 7 (bottom), we have also plotted the average number of phosphorus atoms (N) within a distance r of another phosphorus atom, as obtained by integration of the RDFs. These plots clearly show that the first-neighbor phosphate groups are much closer to each other in the ionic solution than in water. Although neutralizing Na^+ counterions are also present around the SSM in water, their screening ability decreases at their smaller concentrations.

The results in Figure 7 confirm the hypothesis that the presence of electrolytes provides better stabilization of the PEG-ylated SSM by decreasing the Coulombic repulsion of the PO_4^- groups and allowing more monomers to be accommodated in the SSM. Our MD simulations also show that PEG can further stabilize the SSM by forming stable counterion configurations close to the PO_4^- groups. While in our relatively short simulations we observed only single Na^+ ions locked by PEG chains close to the PO_4^- groups (inset in Figure 7 left), these Na^+ configurations may be more common in real systems.

3.6. Effect of the Ionic Concentration on the Micelle Morphology. The sizes and morphologies of self-assembled molecular aggregates are controlled by the monomer[51,52] and solvent properties.[3,53,54] The morphology is determined by the packing of alkane blocks within the aggregate core, which is characterized by the packing parameter $p = v/a_0 l_c$, where v is the volume of the alkane block, a_0 is the effective area per headgroup at which the interaction energy per monomer is minimized, and l_c is the critical length of the alkane block.[32] If the effective size of the headgroup decreases, p grows and the aggregate becomes less spherical.[32] In the SSMs formed by solvated DSPE−PEG_{2000} monomers, a_0 decreases with better screening of the PO_4^- groups, and the SSM morphology changes from spherical (pure water: small p) to oblate (ionic solution: larger p). Notably, as p increases, the SSM grows and the micelle core develops a cavity (see Figure 3h) that potentially can be filled by other molecules. The SSM morphology thus also depends on the filling of its potentially hollow core.

When the solution is varied in a more significant manner, the aggregates can undergo dramatic changes. For example, adding acids or salts to aqueous solutions of asymmetric polystyrene and poly(acrylic acid) diblock copolymers can result in a change in the aggregate morphologies from spherical micelles to rods and vesicles.[3] The presence of acids or ions can either reduce the number of ionic groups in the corona or screen the electrostatic repulsions between these ionic groups, both of which result in increased N_{agg}.

3.7. Effect of the Lipid Concentration on the Micelle Size. In Figure 1, we showed that the average micelle size changes in buffer, as d_h = 15−8 nm at monomer concentrations of c = 5−40 mM. At the same time, the SSM size slightly increases in water for c = 5−40 mM in the approximate range $d_h \approx 3-6$ nm. The sizes of micelles formed in dilute monomer solutions are usually relatively independent of the monomer concentration.[32] However, in the 40 mM DSPE−PEG_{2000} solution, the average distances between the PEG coronas of two neighboring 10- and 90-monomer SSMs are both ~2 nm. These small intermicellar distances are directly visible in the 40 mM monomer solution in water (Figure 2 right).

In buffer solutions, intermicellar interactions are well-screened at small monomer concentrations. At increased monomer concentrations, screening of intermicellar repulsions becomes less effective because of the reduction in the number of counterions per negative headgroup. At the same time, intermicellar distances become smaller and ionic clouds of neighboring micelles overlap, leading to intermicellar coupling and partial micelle destabilization, where the micellar sizes might change. This might explain why at c = 40 mM, the micelle sizes in water ($d_h \approx 5$ nm; $N_{agg} < 8$) and

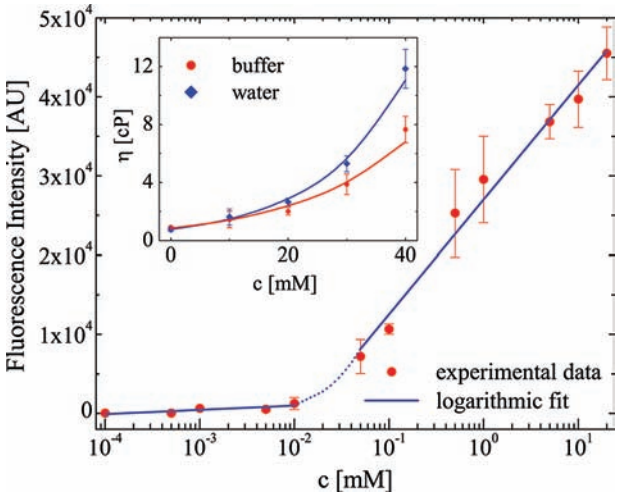

Figure 8. Fluorescence intensity of the DPH probe vs the DSPE−PEG_{2000} concentration in pure water. Solid lines represent fits to the data points using the logarithmic function $I = I_0 \ln(c_{red}) + I_1$, where I is the fluorescence intensity, $c_{red} = c/(1\ mM)$ is the unitless lipid concentration, and I_0 and I_1 give the slope and the intercept, respectively. The fitting parameters were found to be $I_0 = 233$, $I_1 = 2051$ and $I_0 = 6282$, $I_1 = 26{,}999$ for the first ($c < 0.01$ mM) and second ($c > 0.05$ mM) concentration regimes, respectively. The two fit lines are connected by a guiding dashed line. The inset shows the viscosity (η) of the DSPE−PEG_{2000} solution vs lipid concentration in pure water (blue ◆) and HEPES-buffered saline (red ●). Fits to the data using the exponential function $\eta = \eta_0 e^{kc}$ are represented by the corresponding lines. The obtained fit parameters were $\eta_0 = 0.76$ cP, $k = 0.067\ mM^{-1}$ and $\eta_0 = 0.84$ cP, $k = 0.052\ mM^{-1}$ for the water and buffer solutions, respectively.

ionic solution ($d_h \approx 8$ nm; $N_{agg} \approx 15-20$) are similar (Figure 1d, h and Table 1).

3.8. Effect of the Solvent on CMC. In Figure 8, we show how the observed fluorescence intensity of a 1,6-diphenyl-1,3,5-hexatriene (DPH) probe depends on the lipid concentration in water. The concentration at which the fluorescence intensity starts to grow signals the presence of micelles and gives the CMC. The obtained CMC values of 10−20 μM for DSPE−PEG_{2000} in water are in excellent agreement with the previously measured CMC values of 10−25 μM[55] and ∼10 times higher than those obtained in HEPES-buffered saline, $c = 0.5-1.0$ μM.[14] The observed CMC decreases with increasing ionic strength of the solvent, in agreement with the results of previous studies.[26] This CMC decrease is predominantly caused by the increased screening of the charged headgroups, leading to better stabilization of the micelles formed.[56] Another factor that may decrease the CMC of DSPE−PEG_{2000} in the ionic solution could be the smaller number of water molecules available to solubilize DSPE−PEG_{2000} when the water is shared between phospholipids and ions.[57]

3.9. Effect of the Lipid Concentration and Solvent on the Solution Viscosity. Our measurements on DSPE−PEG_{2000} dispersions in pure water and HEPES-buffered saline show that their viscosities increase with increasing lipid concentration (Figure 8 inset). In addition, the viscosity of the pure water solution is higher at every DSPE−PEG_{2000} monomer concentration and increases at a higher rate than that of the buffer solution. These trends can be understood on the basis of Figure 2, where we showed that in 40 mM DSPE−PEG_{2000} solutions, neighboring SSMs can easily come in contact through their PEG coronas. Therefore, the probability of SSM interactions increases rapidly with the lipid concentration, which explains the rapid growth in the viscosity. The slower increase in viscosity in buffer can be explained by the presence of fewer, larger, and more separated micelles.

4. CONCLUSION

We have experimentally and theoretically characterized DSPE−PEG_{2000} assemblies in pure water and HEPES-buffered saline. We have found that the structural and dynamical properties of SSMs strongly depend on the lipid concentration and the solvent medium. The SSM size (aggregation numbers) increases and the CMC decreases with increasing ionic strength (in buffer), as the repulsions between negatively charged phosphate groups are better stabilized by counterion screening in buffered solutions. Our simulations have revealed that the inflatable SSM core, complex ionic interface, and highly fluctuating corona form suitable nesting sites for drugs and other carried molecules. The observed behavior of DSPE−PEG_{2000} in aqueous solutions is of crucial importance for the design of new nanomedicines and other nanoconstructs with versatile applications.

■ ASSOCIATED CONTENT

Ⓢ Supporting Information. Complete ref 41, materials, and experimental and computational methods. This material is available free of charge via the Internet at http://pubs.acs.org.

■ AUTHOR INFORMATION

Corresponding Author

pkral@uic.edu; hayat@uic.edu

Author Contributions

⊥These authors contributed equally.

■ ACKNOWLEDGMENT

This study was supported in part by a grant from the National Institutes of Health (R01CA12797). This investigation was conducted in a facility constructed with support from the NIH National Center for Research Resources through Research Facilities Improvement Program Grant C06RR15482. L.V. acknowledges support from a UIC Dean Scholar Award, and A.M. acknowledges support from UIC Herbert E. Paaren Summer and Academic Year Research Scholarships. The simulations were performed with the NERSC, NCSA, and CNM supercomputers.

■ REFERENCES

(1) Hristova, K.; Needham, D. *Macromolecules* **1995**, *28*, 991–1002.
(2) Belsito, S.; Bartucci, R.; Montesano, G.; Marsh, D.; Sportelli, L. *Biophys. J.* **2000**, *78*, 1420–1430.
(3) Zhang, L.; Yu, K.; Eisenberg, A. *Science* **1996**, *272*, 1777–1779.
(4) Patra, N.; Král, P. *J. Am. Chem. Soc.* **2011**, *133*, 6146–6149.
(5) Johnsson, M.; Edwards, K. *Biophys. J.* **2003**, *85*, 3839–3847.
(6) Jones, M. N. *Adv. Colloid Interface Sci.* **1995**, *54*, 93–128.
(7) Kaler, E. W.; Murthy, A. K.; Rodrigues, B. E.; Zasadzinski, J. A. *Science* **1989**, *245*, 1371–1374.
(8) Luo, L.; Eisenberg, A. *J. Am. Chem. Soc.* **2001**, *123*, 1012–1013.
(9) Nagle, J. F.; Tristram-Nagle, S. *Biochim. Biophys. Acta* **2000**, *1469*, 159–195.
(10) van Meer, G.; Voelker, D. R.; Feigenson, G. W. *Nat. Rev. Mol. Cell. Biol.* **2008**, *9*, 112–124.
(11) Titov, A.; Král, P.; Pearson, R. *ACS Nano* **2010**, *4*, 229–234.
(12) Zalipsky, S. *Bioconjugate Chem.* **1995**, *6*, 150–165.

(13) Koo, O. M.; Rubinstein, I.; Önyüksel, H. *Nanomedicine* **2005**, *1*, 193–212.
(14) Ashok, B.; Arleth, L.; Hjelm, R. P.; Rubinstein, I.; Önyüksel, H. *J. Pharm. Sci.* **2004**, *93*, 2476–2487.
(15) Allen, T. M.; Hansen, C.; Martin, F.; Redemann, C.; Yau-Yong, A. *Biochim. Biophys. Acta* **1991**, *1066*, 29–36.
(16) Maruyama, K.; Yuda, T.; Okamoto, A.; Kojima, S.; Suginaka, A.; Iwatsuru, M. *Biochim. Biophys. Acta* **1992**, *1128*, 44–49.
(17) Harvie, P.; Wong, F. M. P.; Bally, M. B. *J. Pharm. Sci.* **2000**, *89*, 652–663.
(18) Shi, N.; Pardridge, W. M. *Proc. Natl. Acad. Sci. U.S.A.* **2000**, *97*, 7567–7572.
(19) Zhang, Y.; Boado, R. J.; Pardridge, W. M. *Pharm. Res.* **2003**, *20*, 1779–1785.
(20) Welsher, K.; Liu, Z.; Sherlock, S. P.; Robinson, J. T.; Chen, Z.; Daranciang, D.; Dai, H. *Nat. Nanotechnol.* **2009**, *4*, 773–780.
(21) Bianco-Peled, H.; Dori, Y.; Schneider, J.; Sung, L.-P.; Satija, S.; Tirrell, M. *Langmuir* **2001**, *17*, 6931–6937.
(22) Borden, M. A.; Martinez, G. V.; Ricker, J.; Tsvetkova, N.; Longo, M.; Gillies, R. J.; Dayton, P. A.; Ferrara, K. W. *Langmuir* **2006**, *22*, 4291–4297.
(23) Lozano, M. M.; Longo, M. L. *Langmuir* **2009**, *25*, 3705–3712.
(24) Lukyanov, A. N.; Torchilin, V. P. *Adv. Drug Delivery Rev.* **2004**, *56*, 1273–1289.
(25) Torchilin, V. P. *Pharm. Res.* **2007**, *24*, 1–16.
(26) Malmsten, M. *Surfactants and Polymers in Drug Delivery*; Marcel Dekker: New York, 2002.
(27) Onyuksel, H.; Ikezaki, H.; Patel, M.; Gao, X. P.; Rubinstein, I. *Pharm. Res.* **1999**, *16*, 155.
(28) Cesur, H.; Rubinstein, I.; Pai, A.; Önyüksel, H. *Nanomedicine* **2009**, *5*, 178–183.
(29) Koo, O. M.; Rubinstein, I.; Önyüksel, H. *Pharm. Res.* **2011**, *28*, 776–787.
(30) Arleth, L.; Ashok, B.; Önyüksel, H.; Thiyagarajan, J.; Jacob, J.; Hjelm, R. P. *Langmuir* **2005**, *21*, 3279–3290.
(31) Krishnadas, A.; Rubinstein, I.; Önyüksel, H. *Pharm. Res.* **2003**, *20*, 297–302.
(32) Israelachvili, J. *Intermolecular and Surface Forces*, 2nd ed.; Academic Press: New York, 1992.
(33) Thévenot, C.; Grassl, B.; Bastiat, G.; Binana, W. *Colloids Surf., A* **2005**, *252*, 105–111.
(34) Yoshii, N.; Iwahashi, K.; Okazaki, S. *J. Chem. Phys.* **2006**, *124*, No. 184901.
(35) Marrink, S. J.; Tieleman, D. P.; Mark, A. E. *J. Phys. Chem. B* **2000**, *104*, 12165–12173.
(36) Bruce, C. D.; Berkowitz, M. L.; Perera, L.; Forbes, M. D. E. *J. Phys. Chem. B* **2002**, *106*, 3788–3793.
(37) Shang, B. Z.; Wang, Z.; Larson, R. G. *J. Phys. Chem. B* **2008**, *112*, 2888–2900.
(38) Tieleman, D. P.; van der Spoel, D.; Berendsen, H. J. C. *J. Phys. Chem. B* **2000**, *104*, 6380–6388.
(39) Kuramochi, H.; Andoh, Y.; Yoshii, N.; Okazaki, S. *J. Phys. Chem. B* **2009**, *113*, 15181.
(40) Phillips, J. C.; Braun, R.; Wang, W.; Gumbart, J.; Tajkhorshid, E.; Villa, E.; Chipot, C.; Skeel, R. D.; Kalé, L.; Schulten, K. *J. Comput. Chem.* **2005**, *26*, 1781–1802.
(41) MacKerell, A. D.; et al. *J. Phys. Chem. B.* **1998**, *102*, 3586–3616.
(42) Lee, H.; Venable, R. M.; MacKerell, A. D., Jr.; Pastor, R. W. *Biophys. J.* **2008**, *95*, 1590–1599.
(43) Johnsson, M.; Hansson, P.; Edwards, K. *J. Phys. Chem. B* **2001**, *105*, 8420–8430.
(44) Lee, H.; de Vries, A. H.; Marrink, S. J.; Pastor, R. W. *J. Phys. Chem. B* **2009**, *113*, 13186–13194.
(45) Almgren, M.; Löfroth, J. E. *J. Colloid Interface Sci.* **1981**, *81*, 486–499.
(46) Mazer, N. A.; Benedek, G. B.; Carey, M. C. *J. Phys. Chem.* **1976**, *80*, 1075–1085.
(47) Schick, M. J.; Atlas, S. M.; Eirich, F. R. *J. Phys. Chem.* **1962**, *66*, 1326–1333.
(48) Garbuzenko, O.; Zalipsky, S.; Qazen, M.; Barenholz, Y. *Langmuir* **2005**, *21*, 2560–2568.
(49) Takeoka, S.; Mori, K.; Ohkawa, H.; Sou, K.; Tsuchida, E. *J. Am. Chem. Soc.* **2000**, *122*, 7927–7935.
(50) Humphrey, W.; Dalke, A.; Schulten, K. *J. Mol. Graphics* **1996**, *14*, 33–38.
(51) Antonietti, M.; Heinz, S.; Schmidt, M.; Rosenauer, C. *Macromolecules* **1994**, *27*, 3276–3281.
(52) van Hest, J. C. M.; Delnoye, D. A. P.; Baars, M. W. P. L.; van Genderen, M. H. P.; Meijer, E. W. *Science* **1995**, *268*, 1592–1595.
(53) Yu, Y.; Eisenberg, A. *J. Am. Chem. Soc.* **1997**, *119*, 8383–8384.
(54) Choucair, A.; Eisenberg, A. *Eur. Phys. J.* **2003**, *10*, 37–44.
(55) Priev, A.; Zalipsky, S.; Cohen, R.; Barenholz, Y. *Langmuir* **2002**, *18*, 612–617.
(56) Borisov, O. V.; Zhulina, E. B. *Macromolecules* **2002**, *35*, 4472–4480.
(57) Moreira, L.; Firoozabadi, A. *Langmuir* **2010**, *26*, 15177–15191.